Die Grenzen der Chemie neu ausloten?
It takes
#HumanChemistry

Wir suchen kreative Chemikerinnen und Chemiker, die mit uns gemeinsam neue Wege gehen wollen – mit Fachwissen, Unternehmertum und Kreativität für innovative Lösungen. Informieren Sie sich unter:

evonik.de/karriere

EVONIK
Leading Beyond Chemistry

Check for updates

ADVANCED MATERIALS
www.advmat.de

Two-Photon 3D Laser Printing Inside Synthetic Cells

Tobias Abele, Tobias Messer, Kevin Jahnke, Marc Hippler, Martin Bastmeyer,
Martin Wegener, and Kerstin Göpfrich*

Toward the ambitious goal of manufacturing synthetic cells from the bottom up, various cellular components have already been reconstituted inside lipid vesicles. However, the deterministic positioning of these components inside the compartment has remained elusive. Here, by using two-photon 3D laser printing, 2D and 3D hydrogel architectures are manufactured with high precision and nearly arbitrary shape inside preformed giant unilamellar lipid vesicles (GUVs). The required water-soluble photoresist is brought into the GUVs by diffusion in a single mixing step. Crucially, femtosecond two-photon printing inside the compartment does not destroy the GUVs. Beyond this proof-of-principle demonstration, early functional architectures are realized. In particular, a transmembrane structure acting as a pore is 3D printed, thereby allowing for the transport of biological cargo, including DNA, into the synthetic compartment. These experiments show that two-photon 3D laser microprinting can be an important addition to the existing toolbox of synthetic biology.

1. Introduction

Bottom-up synthetic biology is a growing field at the interface of biology and materials science with the visionary aim to construct a functional cell from molecular building blocks.[1–3] Toward this goal, several techniques have become available to assemble cell-sized giant unilamellar lipid vesicles (GUVs) as mimics of cellular compartments.[4–9] Versatile synthetic and natural components have been reconstituted inside GUVs to achieve important functions of cells, such as compartment replication,[10] energy generation[11,12] or transmembrane trafficking.[6,13,14] However, the highly controlled spatio-temporal organization that characterizes living cells remains hitherto unachieved in today's synthetic counterparts.

Introducing space-filling structures into already formed compartments appears to be in contradiction with the barrier defining the compartment volume. Hence, the internal organization of synthetic cells typically relies on self-assembly, which limits the complexity of the achievable end result. Especially when it comes to the recombination of several functional modules, self-assembly can be impaired due to undesired interactions or incompatible environmental requirements.[2,15] Early attempts have been made to address this shortcoming by the sequential addition of components by injection through the lipid membrane[5,16] or vesicle fusion.[17–20] While such strategies can increase the achievable complexity, they also disrupt the membrane and change the compartment volume. Alternatively, a lipid vesicle can be formed around a preformed element, which has led to promising results.[4,21,22] However, this "inside-out" assembly strategy for synthetic cells neglects the role of confinement for the assembly process itself. Therefore, strategies for the non-destructive alteration of internal organization of the compartment and the addition of large structures inside compartments are highly desirable. Toward this end, light-triggered actuation of chemical reactions[23–26] and dynamic mechanical response[27,28] opens up exciting directions. Similarly, the light-triggered polymerization of a space-filling hydrogel was realized inside cells[29] and lipid vesicles.[30] Nevertheless, strategies for the assembly of well-defined arbitrary architectures inside preformed compartments are missing in bottom-up synthetic biology, and, more broadly, in 3D manufacturing.

We suggest that two-photon 3D laser printing, as a powerful non-contact printing method, can address this challenge. This approach uses femtosecond optical pulses and two-photon excitation to trigger polymerization only at the desired 3D

T. Abele, K. Jahnke, K. Göpfrich
Biophysical Engineering Group
Max Planck Institute for Medical Research
Jahnstraße 29, 69120 Heidelberg, Germany
E-mail: kerstin.goepfrich@mr.mpg.de

T. Abele, K. Jahnke, K. Göpfrich
Department of Physics and Astronomy
Heidelberg University
69120 Heidelberg, Germany

T. Messer, M. Wegener
Institute of Applied Physics
Karlsruhe Institute of Technology (KIT)
Wolfgang-Gaede-Str. 1, 76131 Karlsruhe, Germany

M. Hippler, M. Wegener
Institute of Nanotechnology
Karlsruhe Institute of Technology (KIT)
Hermann-von-Helmholtz-Platz 1, 76344 Eggenstein-Leopoldshafen, Germany

M. Hippler, M. Bastmeyer
Zoological Institute
Karlsruhe Institute of Technology (KIT)
Fritz-Haber-Weg 4, 76131 Karlsruhe, Germany

M. Bastmeyer
Institute for Biological and Chemical Systems - Biological Information Processing (IBCS-BIP)
Karlsruhe Institute of Technology (KIT)
Hermann-von-Helmholtz-Platz 1, 76344 Eggenstein-Leopoldshafen, Germany

The ORCID identification number(s) for the author(s) of this article can be found under https://doi.org/10.1002/adma.202106709.

© 2021 The Authors. Advanced Materials published by Wiley-VCH GmbH. This is an open access article under the terms of the Creative Commons Attribution License, which permits use, distribution and reproduction in any medium, provided the original work is properly cited.

DOI: 10.1002/adma.202106709

position.[31] Progress in femtosecond two-photon polymerization was crucial for the rapid layer-by-layer manufacturing of almost arbitrary shapes on the nano- and micrometer scale.[32,33] Whereas hydrogel-based microstructures have been demonstrated by various groups,[34,35] 3D laser printing in a water-soluble photoresist and printing in the presence of cells is increasingly gaining attention.[36–41]

Here, we use two-photon 3D laser printing for the manufacturing of complex 3D architectures inside GUVs. Furthermore, we characterize the diffusive influx of photoresist components into GUVs and confirm that the printing process itself does not damage the lipid bilayer. Going beyond proof-of-principle printing demonstrations, we realize functional transmembrane pores for the transport of biological cargo into GUVs.

2. Results and Discussion

2.1. 3D Laser Printing of Hydrogel Structures Inside GUVs

Figure 1 illustrates the proposed concept to write custom-shaped 3D structures inside preformed compartments by femtosecond two-photon polymerization. Importantly, two-photon polymerization allows to trigger the polymerization at a desired 3D position, leading to a polymerized volume element, which is referred to as the voxel. In particular, two-photon absorption of the photoinitiator produces free radicals, which, in turn, initiate the radical polymerization of the resist monomers. This offers the unique yet unexplored possibility to print inside a preformed compartment in a non-destructive manner with full spatio-temporal control. While the general concept to print inside compartments may become applicable in diverse fields of science and technology, we set out to demonstrate its relevance for bottom-up synthetic biology. As an initial proof of principle, we successfully demonstrated printing of arbitrary objects inside water-in-oil droplets (Figure S1, Supporting Information). Nevertheless, synthetic cells enclosed by a lipid bilayer better mimic cellular membranes, which is why we chose GUVs as a more relevant compartment type.[42–44] Printing inside GUVs is especially challenging due to their mechanical instability[2] and the chemical photoresist requirements. A suitable resist has to fulfill several criteria: i) It has to be soluble in an aqueous solvent. ii) The encapsulation into GUVs has to be possible at sufficiently high concentrations without compromising the GUV stability. iii) Ideally, it should be possible to develop the structures after printing, which requires suitable strategies to remove the photoinitiator and unpolymerized resist components from the GUV lumen. iv) The printing process itself should not cause movement or destruction of the GUV.

We chose commonly used water-soluble resist components (Requirement (i)), namely the photoinitiator lithium phenyl-2,4,6-trimethylbenzoylphosphinate (LAP), the prepolymer poly(ethylene glycol) diacrylate 575 (PEGDA)[45,46] and the fluorescent acryloxyethyl thiocarbamoyl rhodamine B monomer (Rhodamine B acrylate) for imaging purposes. Additionally, we supplemented the resist with sucrose at a high osmolarity (800×10^{-3} M) to buffer osmotic pressure fluctuations which could damage the GUVs.[17]

Next, we set out to test if Requirements (ii) and (iii) can be fulfilled, that is, if the resist can be brought into the GUV and if excess components can be removed after printing. GUVs were prepared with a conventional lipid composition (99%

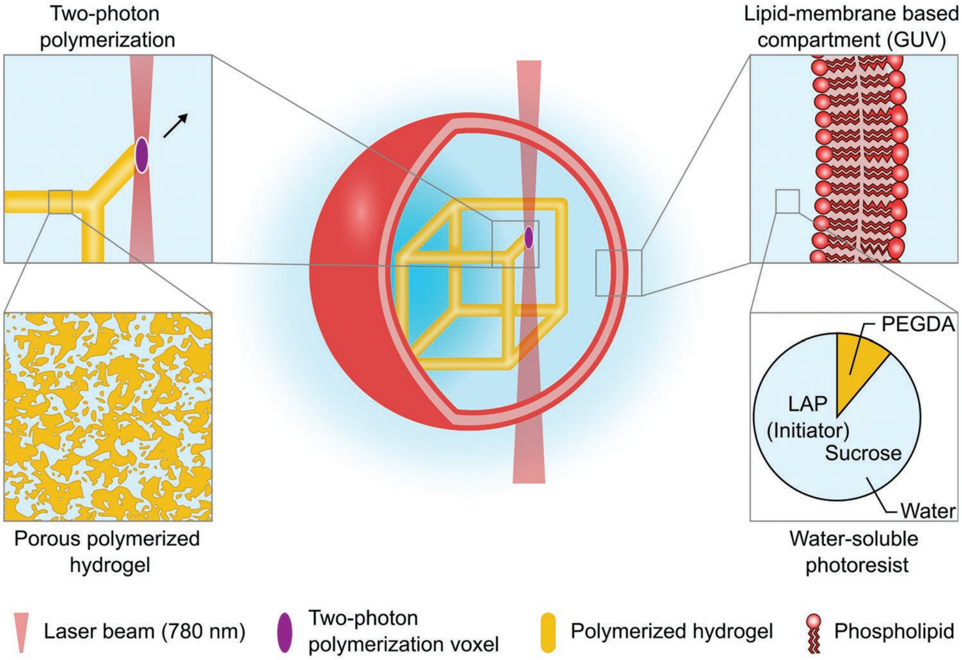
Two-photon polymerization
Lipid-membrane based compartment (GUV)
PEGDA
LAP (Initiator)
Sucrose
Water
Porous polymerized hydrogel
Water-soluble photoresist
Laser beam (780 nm)
Two-photon polymerization voxel
Polymerized hydrogel
Phospholipid

Figure 1. 3D laser printing in synthetic cells. Schematic illustration of a 3D hydrogel cube frame (yellow) as an exemplary object that was written into a preformed giant unilamellar lipid vesicle (GUV, red) by two-photon polymerization. GUVs are micrometer-sized lipid bilayer enclosed compartments often used as synthetic cell models. The nanoporous hydrogel cube frame consists of PEGDA and was formed by local radical polymerization in the presence of the photoinitiator LAP dissolved in aqueous sucrose-containing solution.

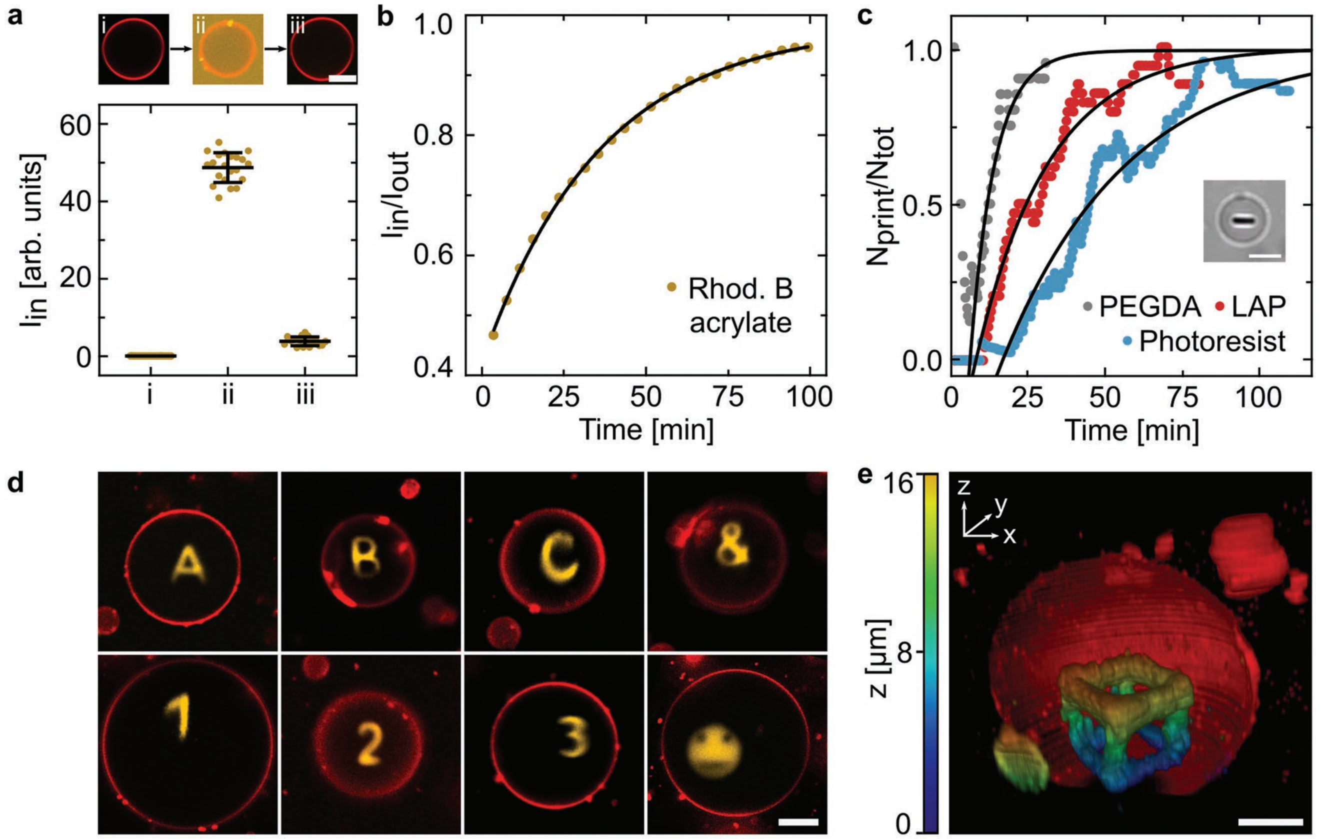

Figure 2. Laser printing of nearly arbitrary 2D and 3D hydrogel structures inside GUVs. a) Representative confocal images of a GUV (red, $\lambda_{ex} = 640$ nm): i) before mixing GUVs with photoresist, ii) 2 h after mixing GUVs with photoresist (yellow, fluorescent component: Rhodoamine B acrylate, $\lambda_{ex} = 561$ nm), and iii) 2 h after diluting the mixture of GUVs and photoresist from (ii) in aqueous sucrose solution. The corresponding quantified fluorescence intensity inside the GUVs, I_{in}, is shown below (n= 17 to n = 25, mean ± standard deviation (s.d.)). Scale bar: 10 µm. b) Ratio of fluorescence intensity inside, I_{in}, and outside, I_{out}, of a GUV as a function of time. An exponential fit (black line) yielded a membrane permeability coefficient for the diffusion of Rhodamine B acrylate into the GUVs of $P = 2.301 \pm 0.016$ nm s^{-1}. c) Membrane permeability of PEGDA, LAP, and the complete photoresist. The membrane permeability was determined by adding the respective components after incubation of the GUVs with the remaining components of the photoresist and quantifying the fraction of successful printing attempts, N_{print}/N_{tot}, inside the GUVs over time. An exponential fit (black line) was used to determine the point in time of 50% success rate. Scale bar: 10 µm. d) Confocal images of printed 2D structures (yellow, $\lambda_{ex} = 561$ nm) inside GUVs (red, $\lambda_{ex} = 640$ nm). Scale bar: 10 µm. e) Color-coded 3D surface reconstruction of confocal images of a 3D printed cube frame inside a 40 µm-sized GUV. Scale bar: 10 µm.

1,2-dioleoyl-sn-glycero-3-phosphocholine (DOPC), 1% ATTO633-1,2-dioleoyl-sn-glycero-3-phosphoethanolamine (DOPE)) using the electroformation method.[9] When mixing GUVs and the photoresist components, confocal imaging revealed the influx of the fluorescent Rhodamine B acrylate across the lipid bilayer membrane into the GUV lumen (**Figure 2**a), equilibrating the concentrations inside and outside of the GUV. Since Rhodamine B acrylate represents the largest component of the photoresist, this finding hints that also the other resist components can be brought into the GUVs by diffusion (Requirement (ii)). Importantly, diffusion of the resist components through the lipid membrane works in both directions. For removal of unpolymerized components, the GUVs immersed in Rhodamine B acrylate are diluted in an osmolarity-matched solution free of photoresist components. The concentration gradient of the resist across the membrane leads to resist efflux from the GUVs until an equilibrium is reached (Figure 2a-iii). Removal of the resist from the GUV lumen provides the possibility to develop encapsulated structures after printing inside the GUV (Requirement (iii)). To gain quantitative insights into the Rhodamine B acrylate influx into GUVs, we measured the fluorescence intensity ratio inside and outside of GUVs, I_{in}/I_{out}, over time, yielding a membrane permeability coefficient of 2.301 ± 0.016 nm s^{-1} (Figure 2b, Note S1, Supporting Information), which is comparable to reported literature values for the permeability of the antibiotic norfloxacin[47] or the charged compound bicarbonate.[48] We were able to polymerize the resist inside the GUV by two-photon 3D laser printing. This observation is a direct proof for the influx of all resist components. As visible in the microscopy image in Figure 2c (see inset), we successfully printed a rod-shaped element into the lumen of the GUV. We used the printing success rate as an indirect way to determine the membrane permeability of the non-fluorescent components. Successful printing attempts were defined as attempts where the desired structure was visible in the bright-field microscope right after printing inside the GUV. For this purpose, PEGDA or LAP was added to GUVs that were pre-incubated with the other resist components. We printed in

GUVs with an average diameter of 26.6 ± 7.9 µm (Figure S2, Supporting Information). Subsequently, we quantified the fraction of successful printing attempts over the course of up to 100 min. We observed increase in the printing success rate over time because of the diffusion of the respective resist component into the GUVs (Figure 2c). Due to their increased surface-to-volume ratio, printing in smaller GUVs was possible at earlier time points (Figure S3, Supporting Information). In most of the unsuccessful printing attempts, the GUV remained intact but no structure appeared inside, likely due to insufficient supply of one of the resist components in the GUV lumen. Importantly, the GUVs did not move during the printing process, despite potential laser heating, once they settled due to gravity in a glucose-sucrose gradient (Requirement (iv)). In more detail, after adding LAP to GUVs, it took 24.27 ± 1.07 min to achieve a 50% printing success rate. Having determined the minimal LAP concentration required for printing (Figure S4, Supporting Information), this yields a membrane permeability of 0.987 ± 0.325 nm s^{-1} (Note S2, Supporting Information). PEGDA was found to diffuse faster across the membrane, such that printing in 50% of the GUVs was already possible after 11.48 ± 0.88 min, corresponding to a membrane permeability of 3.875 ± 1.330 nm s^{-1}. Although LAP is a smaller molecule compared to Rhodamine B acrylate, its membrane permeability is lower. This is likely due to its polarity and negative charge (Figure S5, Supporting Information). When adding PEGDA and LAP at the same time, we achieve a 50% printing success ratio at a later time point after 44.83 ± 2.68 min, potentially due to the increased access resistance. From the permeability coefficients, we were able to determine the concentration of all three resist components inside the GUVs over time according to Fick's law of diffusion (Figure S6, Supporting Information). Most importantly, it should be highlighted that printing was successful in over 88% of the GUVs after 100 min incubation with the resist components. If printing was unsuccessful despite sufficiently long incubation, this was typically the case because the GUV bursted during the printing process. Bursting occurred when the 3D positioning of the polymerization voxel was insufficiently accurate and polymerization was triggered in very close proximity to the lipid bilayer, likely causing lipid oxidation (Figures S7 and S8, Supporting Information).[17]

The high printing success rate encouraged us to print more complex 2D a 3D shapes into GUVs and to visualize them by confocal fluorescence microscopy. Figure 2d shows various 2D hydrogel structures printed inside GUVs, including letters, numbers and symbols. From confocal microscopy data, the feature sizes of the structures were determined to be 1.69 ± 0.14 µm within the *xy*-plane and 7.16 ± 0.61 µm for the *z*-direction, respectively (Figure S9, Supporting Information). In principle, smaller feature sizes are possible, for instance, by printing just one instead of four layers. However this would compromise the structural stability of the printed features with the currently used resist. After printing, the structures freely diffused inside the GUV lumen (Movie S1, Supporting Information) and slowly settled to the bottom of the GUVs due to gravity. This could be exploited for the separation of GUVs that contain printed structures from those that are empty. If required, settling could be avoided either by gentle shaking, by modifying the photoresist such that the polymerized structures are less dense, or by connecting the printed structures to the membrane. We find that we can print at printing speeds ranging from 1 mm s^{-1} to 2 mm s^{-1} in order to manufacture all layers at near-constant position of the structure itself. Capitalizing on the high spatial resolution of femtosecond two-photon polymerization, Figure 2e presents a 3D reconstruction of a 16 µm high 3D cube frame inside a 40 µm GUV.

To summarize this part, we successfully enriched the inner volume of GUVs with photopolymerizable hydrogel components via diffusion across the lipid bilayer and demonstrated the deterministic polymerization of various structures in 2D and 3D inside GUVs. This concept can also be extended to other compartment types like water-in-oil droplets (Figure S1, Supporting Information). Moreover, if lower resolution along the *z*-direction can be tolerated, printing can be achieved with the laser of a confocal microscope or other types of illumination (Figure S10, Supporting Information). This aspect makes printing inside compartments also broadly applicable beyond synthetic biology.

2.2. Lipid Membrane and Hydrogel Properties

Having confirmed that femtosecond two-photon polymerization inside GUVs does not destroy them (Requirement (iv)), we examined the effects of the photoresist and two-photon 3D laser printing process on the lipid bilayer. We thus investigated possible unintentional alterations of the lipid diffusivity, which is a crucial indicator for membrane property changes, such as resist-membrane interactions, oxidation[49] or changes in membrane composition due to the presence of the photoresist in the membrane. First of all, we confirmed with fluorescence recovery after photobleaching (FRAP) measurements (Note S3, Supporting Information,[5]) that the membrane of GUVs containing a printed structure inside their lumen remained diffusive (**Figure 3**a). The fluorescence of the bleached area recovered within seconds. An exponential fit yields the diffusion coefficient D of the lipids for different conditions, namely prior to resist encapsulation, before and after equilibration of the resist concentration inside and outside the GUVs (i.e., 0.25 h and 2 h after adding the photoresist to the GUVs, respectively) and after printing a rod structure inside the GUV lumen (Figure 3b). Directly after addition of the resist (0.25 h), the lipid diffusion coefficient D increased slightly but significantly ($D = 3.455 \pm 0.517$ µm^{2}s^{-1} and $D = 2.887 \pm 0.640$ µm^{2}s^{-1}, respectively, $p = 0.029$), likely due to the imbalanced distribution of the photoresist at this time point. In contrast, 2h after photoresist addition, when the concentrations inside and outside of the GUVs have equilibrated, the lipid diffusion coefficient decreased slightly. This is likely due to the higher viscosity of the solution in the presence of the resist and the presence of resist components in the membrane ($p = 0.004$). Most importantly, the printing process did not affect the diffusion coefficient significantly ($D = 2.129 \pm 0.610$ µm^{2}s^{-1}, $p = 0.133$), fulfilling Requirement (iv).

In order to derive functionality for the printed hydrogels, we investigated their microscopic structure. FRAP experiments confirmed that the hydrogel is polymerized and hence not diffusive (Figure S11, Supporting Information). Atomic force microscopy (AFM) of the polymerized photoresist revealed sub-

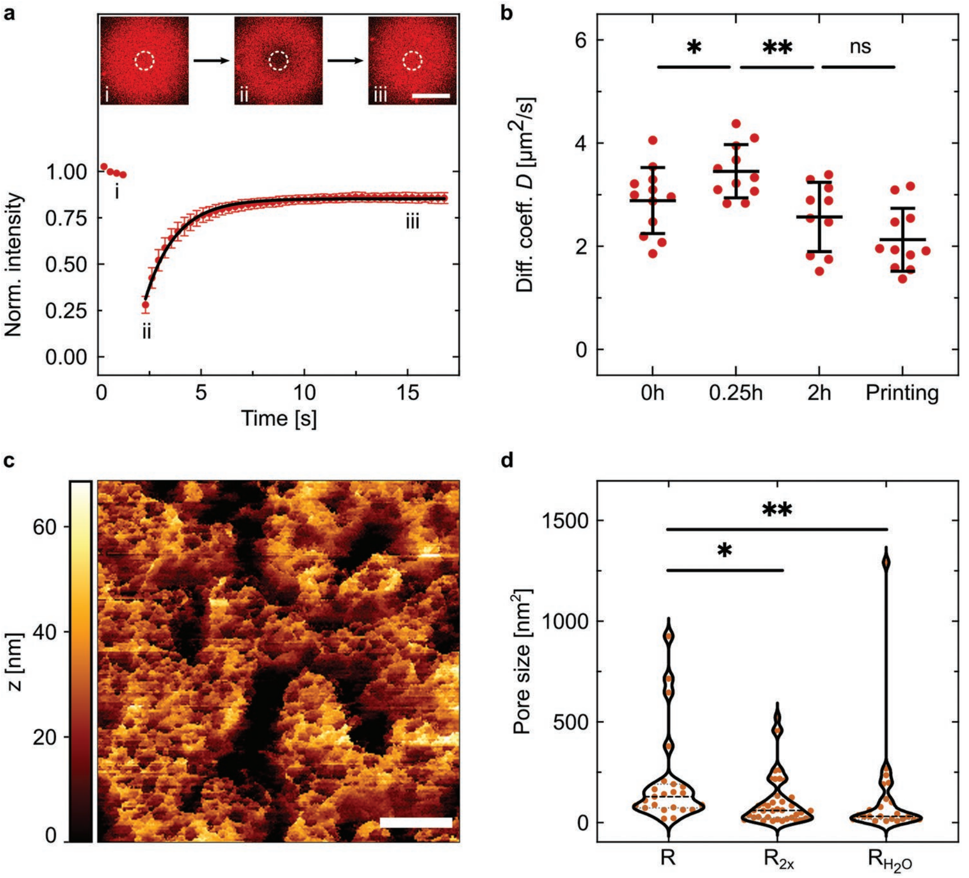

Figure 3. Characterization of the GUV membrane and the printed hydrogel. a) FRAP experiments on GUVs after printing. Confocal fluorescence images of the top plane of a GUV (red, $\lambda_{ex} = 640$ nm): i) before photobleaching of a circular area (white dashed line), ii) directly after photobleaching, and iii) after fluorescence recovery. The normalized mean intensity of the bleaching area is plotted over time. The error bars represent the standard deviation for $n = 12$ GUVs after printing a hydrogel structure into their lumen. An exponential fit (black line) yielded a lipid diffusion coefficient of $D = 2.129 \pm 0.610$ µm s^{-2}, confirming that the membrane remains intact after printing. Scale bar: 10 µm. b) Lipid diffusion coefficients determined by FRAP for GUVs before mixing with photoresist (0 h), 0.25 h after adding GUVs into the photoresist (0.25 h), 2 h after adding GUVs into photoresist (2 h), and for GUVs in the photoresist after printing a rod structure inside their lumen ($n = 10$ to $n = 12$, mean ± s.d.). c) AFM image of a polymerized block of the photoresist used for printing inside GUVs. Scale bar: 200 nm. d) Pore size distribution as determined from AFM images for the polymerized photoresist (R) used for printing inside GUVs, the polymerized photoresist at doubled PEGDA and LAP concentration (R_{2x}), and polymerized photoresist in water without sucrose or glucose (R_{H_2O}).

micron-sized pores inside the hydrogel (Figure 3c). Note that the hydrogel was manufactured with the same resist composition that was present within GUVs after equilibration. We found that the pore size can be tuned by changing the resist concentration as well as the concentration of sucrose (Figure S12, Supporting Information). More specifically, Figure 3d quantifies the pore size distribution of the polymerized photoresist used for printing inside GUVs (R) in comparison to a resist with a twofold increased concentration of PEGDA and LAP (R_{2x}) and a resist without the addition of sucrose and glucose (R_{H_2O}). The surface roughness (Figure S13, Supporting Information) and the pore size of photoresist R is increased significantly in comparison to the resist variations R_{2x} ($p = 0.010$) and R_{H_2O} ($p = 0.005$). This leads to the conclusion that both, the high water content (88.9 vol%) and addition of sugars, which can act as porogens,[50] increase hydrogel porosity in the sub-micron regime.

We can thus conclude that the membrane remains intact after printing and that the polymerized hydrogel is porous. This opens up exciting opportunities for applications of 3D laser printing in lipid vesicles in the context of bottom-up synthetic biology.

2.3. 3D Laser Printing of a Transmembrane Pore

As a first application, we set out to write a transmembrane pore that spans the lipid bilayer. Due to the porous nature of the printed hydrogel, a structure that is written across the membrane should open up a passage for biomolecular cargo as illustrated in **Figure 4**a. At the same time, printing across the membrane sets yet another technological challenge concerning the feasibility and the stability of the GUVs.

Importantly, we found that printing across the lipid membrane is possible without destruction of the GUVs. After two-photon polymerization of the respective area, a hydrogel structure with a diameter of approximately 5 µm clearly spanned the GUV membrane as visible in the bright-field image in

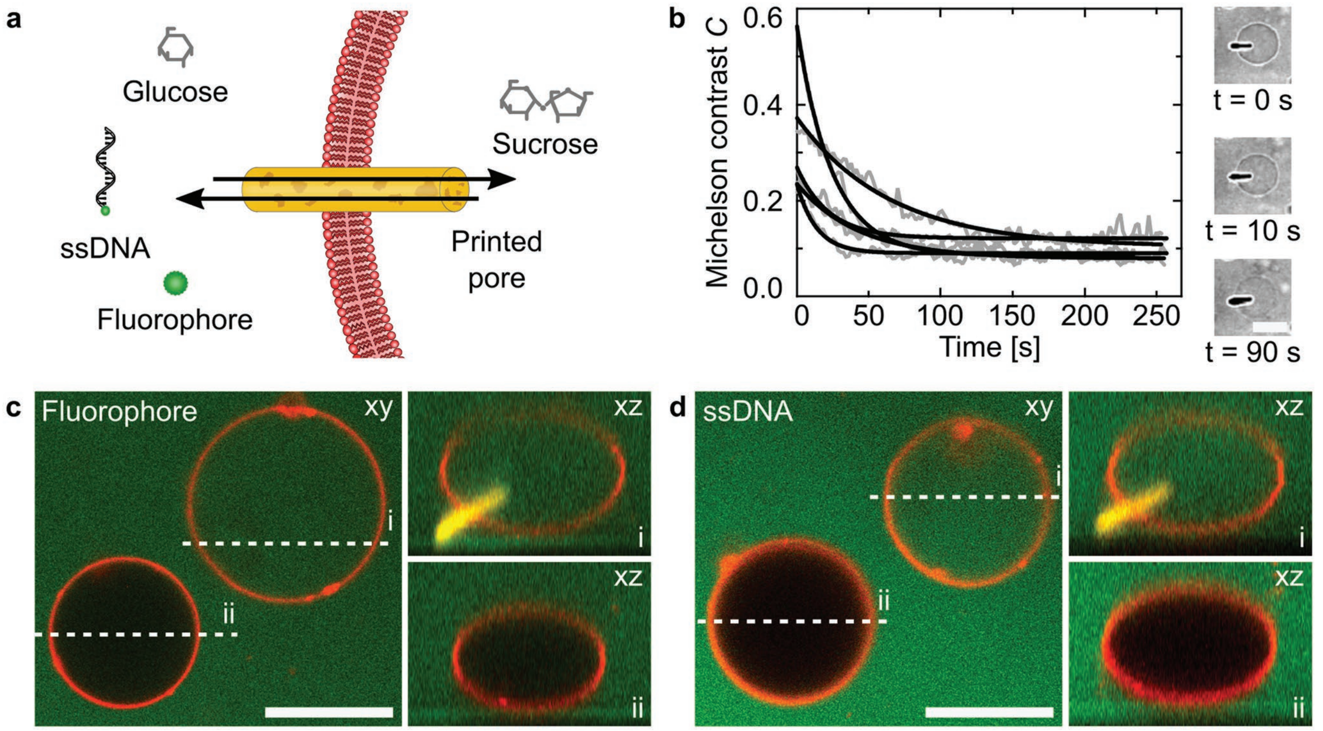

Figure 4. 3D laser printing of a transmembrane-spanning pore across the GUV membrane. a) Schematic illustration of a printed PEGDA hydrogel pore across the lipid membrane of a GUV. The pore allows for the passage of various molecules, including glucose, sucrose, a fluorophore and single-stranded DNA (ssDNA). b) Michelson contrast $C = (I_{\max} - I_{\min})/(I_{\max} + I_{\min})$ for 5 GUVs as a function over time after printing a pore across the membrane. Due to exchange of refractive index influencing molecules sucrose and glucose, the Michelson contrast decreases over time, as displayed in representative bright-field optical images taken at the referenced timepoints of 0 s, 10 s, 90 s after printing the pore. An exponential fit (black line) yielded a pore permeability coefficient of $P = 0.48 \pm 0.25$ µm s^{-1} for the glucose/sucrose exchange. Scale bar: 20 µm. c) Representative confocal images of two adjacent GUVs (red, $\lambda_{ex} = 488$ nm) in the *xy*- (left) and an *xz*-plane (right, as indicated by white dashed lines). i) A hydrogel pore (yellow, $\lambda_{ex} = 561$ nm) was printed into the upper GUV, leading to the influx of the membrane-impermeable fluorophore Alexa Fluor 647 NHS (green, $\lambda_{ex} = 640$ nm). ii) No influx was detected for the adjacent GUV without the printed pore. Scale bar: 20 µm. d) Representative confocal images of two adjacent GUVs as described in (c), demonstrating that also a 13-nucleotide-long single-stranded DNA (green, labeled with Atto647N, $\lambda_{ex} = 640$ nm) can diffuse into the GUV across the printed pore. Printing of transmembrane-spanning structures was successful in 41.5% of the attempts ($n = 59$). Scale bar: 20 µm.

Figure 4b. When printing across the membrane, illumination of the photoinitiator produces free radicals in close proximity to the lipid tails. We confirmed that this causes lipid oxidation (Figures S7 and S8, Supporting Information), which, in turn is known to facilitate pore formation.[17] Transient lipid pores possibly expand and merge such that resist components that are present in the membrane can polymerize. Note that the use of two-photon illumination allows to spatially control production of free radicals (Figure S8, Supporting Information),[51] which are immediately consumed for the polymerization process.[51] Therefore, lipid oxidation is unlikely to occur when structures are printed inside the compartment. Membrane-spanning structures could be printed in 41.5% of our printing attempts (n = 59). In the other cases GUVs bursted and collapsed. Increasing the laser intensity by 10% resulted in a decreased success ratio of 32% (n = 50), enhancing the probability of GUV destruction.

To test whether the printed transmembrane structure acts as a pore and enables substance exchange between the interior and the environment of the GUV, we made use of the glucose-sucrose gradient across the GUV membrane. The refractive-index mismatch between the glucose outside and the sucrose solution inside the GUV causes an optical contrast which disappears if glucose and sucrose are exchanged across the lipid membrane. Figure 4b plots the decrease of the Michelson contrast $C = (I_{\max} - I_{\min})/(I_{\max} + I_{\min})$ over time after two-photon polymerization of a rod structure across the lipid bilayer (Movie S2, Supporting Information), with $I_{\max}$ and $I_{\min}$ being the maximum and minimum intensity value across the lipid bilayer, respectively (n = 5). The decrease of the optical contrast indicates the equilibration of the sucrose and glucose concentrations inside and outside of the GUVs. This clearly demonstrates that the nanoporous membrane-spanning hydrogel acts as a channel to enable transport across the lipid bilayer. Exponential fits yielded a permeability coefficient of the pores for sucrose and glucose of 0.48 ± 0.25 µm s^{-1}. Negligible decrease in the Michelson contrast occurred for GUVs when no pore was printed (Figure S14, Supporting Information) as expected due to the low membrane permeability of sugars.[52]

Next, we tested if our pores can transport larger and charged molecular cargo. Figure 4c shows the influx of the fluorophore Alexa Fluor 647 NHS ester into GUVs containing a pore (i), whereas it was excluded from an adjacent GUV without a pore (ii). In the *xz*-plane, the printed pore is clearly visible for GUV (i). Moving on to biologically relevant macromolecular cargo, Figure 4d shows the influx of single-stranded DNA across a printed hydrogel pore. Note that the printing settings and the photoresist composition were kept the same. Therefore, the porosity of the hydrogel remains unaltered within statistical variations. Again, an adjacent GUV without a pore does not show DNA import, highlighting the advantage of 3D laser printing to induce transport with full spatio-temporal control at the single-GUV level.

Our PEGDA-pore is considerably different from a native transmembrane protein—not just in chemical composition but also considering its architecture and dimensions. Instead of a hollow membrane-spanning cylindrical pore, the printed pore features a nanoporous hydrogel that forms a mesh-architecture more like FG-repeats in the nuclear pore complex.[53] Moreover, the printed transmembrane pore is likely the largest man-made transmembrane pore to date, exceeding the size of the nuclear pore complex.[53] In particular, large pores capable of transporting macromolecules across the membrane are often difficult to isolate and to reconstitute in synthetic cells. With their engineerable properties, printed hydrogel pores may address a challenge in bottom-up synthetic biology, since the reconstitution of protein pores that can transport large macromolecular cargo remains a bottleneck.

3. Conclusion

Rebuilding biological cells requires the technological ability of intracellular structuring and organization. Our work realized the deterministic assembly of molecules into nearly arbitrary 2D and 3D shapes inside GUVs by using femtosecond two-photon 3D laser printing. Importantly, we proved that neither the photoresist nor the two-photon polymerization process impair the lipid bilayer. Their mechanical fragility renders GUVs one of the most challenging compartment types. We already demonstrated that it is possible to extend the concept to emulsion droplets and are therefore confident that it will be possible to print in various compartment types, such as polymersomes, proteinosomes or coacervates, as long as the materials allow for light propagation at the required wavelength. Although we were able to encapsulate the resist by diffusion, which has the advantage that the structures can be developed after printing, resist encapsulation during compartment formation or by injection is in principle also possible. Additionally, we characterized the pore size of polymerized hydrogels and investigated their tunability by changing concentrations of the photoresist components. The material properties can, in principle, be adapted further by using functionalized and stimulus-responsive monomers or hybrid materials to realize variable functions, including compartmentalization and deterministic intracellular release of biological molecules or to mimic the cytoskeleton. Eventually, we achieved the printing of a transmembrane pore for the transport of biological cargo. The pore size is freely tuneable by tuning the size of the printed structure or the hydrogel mesh size which offers the unique possibility to achieve selective cargo transport across scales. Since the physical and the chemical properties of the hydrogel can be altered by varying the resist composition, it will be possible to make custom pores for specific analytes. In particular, adjusting the porosity of the nanoporous hydrogel opens up avenues to tune the transport rates. Moreover, the printing process provides full spatio-temporal control over the transport such that complex reaction networks can be realized in femtoliter compartments and synthetic cell communities. It is remarkable that the GUV remains intact when a structure is printed across its membrane. Ultimately, 3D laser printing could be transferred into biological cells to establish cell polarity, for cell actuation and local force application or for local expansion microscopy. We envision that 3D laser printing inside biological compartments will contribute to the toolbox of synthetic biology, which may, in the future, lead to a fully 3D printed synthetic cell.

Supporting Information

Supporting Information is available from the Wiley Online Library or from the author.

Acknowledgements

The authors thank Ali Aghebat Rafat for support with the AFM experiments and Sebastian Fabritz and the Mass Spectrometry Facility at the Max Planck Institute for Medical Research for performing mass spectrometry experiments. All the authors acknowledge funding from the Deutsche Forschungsgemeinschaft (DFG, German Research Foundation) under Germany's Excellence Strategy via the Excellence Cluster 3D Matter Made to Order (EXC-2082/1 – 390761711). T.A., K.J., and K.G. acknowledge the Max Planck Society for its general support. K.J. thanks the Carl Zeiss Foundation for financial support. T.M. acknowledges funding by the Karlsruhe School of Optics and Photonics (KSOP). T.M., M.H., M.B. and M.W. acknowledge additional support by the Helmholtz program "Materials Systems Engineering".

Open access funding enabled and organized by Projekt DEAL.

Conflict of Interest

A patent application has been filed on the present results.

Data Availability Statement

The data that support the findings of this study are openly available in heiDATA, the Open Research Data institutional repository for Heidelberg University, at https://doi.org/10.11588/data/PUKJCV, reference number [54].

Keywords

3D laser printing, additive manufacturing, bottom-up synthetic biology, direct laser writing, giant unilamellar lipid vesicles, PEGDA hydrogel, transmembrane pores

Received: August 25, 2021
Revised: November 17, 2021
Published online:

[1] H. Mutschler, T. Robinson, T.-Y. D. Tang, S. Wegner, *ChemBioChem* **2019**, *20*, 2533.
[2] K. Göpfrich, I. Platzman, J. P. Spatz, *Trends Biotechnol.* **2018**, *36*, 938.
[3] P. Schwille, J. Spatz, K. Landfester, E. Bodenschatz, S. Herminghaus, V. Sourjik, T. J. Erb, P. Bastiaens, R. Lipowsky,

A. Hyman, P. Dabrock, J.-C. Baret, T. Vidakovic-Koch, P. Bieling, R. Dimova, H. Mutschler, T. Robinson, T.-Y. D. Tang, S. Wegner, K. Sundmacher, *Angew. Chem., Int. Ed.* **2018**, *57*, 13382.

[4] K. Göpfrich, B. Haller, O. Staufer, Y. Dreher, U. Mersdorf, I. Platzman, J. P. Spatz, *ACS Synth. Biol.* **2019**, *8*, 937.

[5] M. Weiss, J. P. Frohnmayer, L. T. Benk, B. Haller, J.-W. Janiesch, T. Heitkamp, M. Börsch, R. B. Lira, R. Dimova, R. Lipowsky, E. Bodenschatz, J.-C. Baret, T. Vidakovic-Koch, K. Sundmacher, I. Platzman, J. P. Spatz, *Nat. Mater.* **2017**, *17*, 89.

[6] L. V. de Cauter, F. Fanalista, L. van Buren, N. D. Franceschi, E. Godino, S. Bouw, C. Danelon, C. Dekker, G. H. Koenderink, K. A. Ganzinger, *ACS Synth. Biol.* **2021**, *10*, 1690.

[7] S. Deshpande, Y. Caspi, A. E. C. Meijering, C. Dekker, *Nat. Commun.* **2016**, *7*, 10447.

[8] B. C. Buddingh', J. C. M. van Hest, *Acc. Chem. Res.* **2017**, *50*, 769.

[9] M. I. Angelova, D. S. Dimitrov, *Faraday Discuss. Chem. Soc.* **1986**, *81*, 303.

[10] K. Kurihara, M. Tamura, K. ichiroh Shohda, T. Toyota, K. Suzuki, T. Sugawara, *Nat. Chem.* **2011**, *3*, 775.

[11] K. Y. Lee, S.-J. Park, K. A. Lee, S.-H. Kim, H. Kim, Y. Meroz, L. Mahadevan, K.-H. Jung, T. K. Ahn, K. K. Parker, K. Shin, *Nat. Biotechnol.* **2018**, *36*, 530.

[12] T. Pols, H. R. Sikkema, B. F. Gaastra, J. Frallicciardi, W. M. Śmigiel, S. Singh, B. Poolman, *Nat. Commun.* **2019**, *10*, 4239.

[13] S. Krishnan, D. Ziegler, V. Arnaut, T. G. Martin, K. Kapsner, K. Henneberg, A. R. Bausch, H. Dietz, F. C. Simmel, *Nat. Commun.* **2016**, *7*, 12787.

[14] A. Ohmann, K. Göpfrich, H. Joshi, R. F. Thompson, D. Sobota, N. A. Ranson, A. Aksimentiev, U. F. Keyser, *Nucleic Acids Res.* **2019**, *47*, 11441.

[15] L. Pasotti, N. Politi, S. Zucca, M. G. C. D. Angelis, P. Magni, *PLoS ONE* **2012**, *7*, e39407.

[16] A. Jesorka, N. Stepanyants, H. Zhang, B. Ortmen, B. Hakonen, O. Orwar, *Nat. Protoc.* **2011**, *6*, 791.

[17] Y. Dreher, K. Jahnke, E. Bobkova, J. P. Spatz, K. Göpfrich, *Angew. Chem., Int. Ed.* **2021**, *60*, 10661.

[18] Y.-H. M. Chan, B. van Lengerich, S. G. Boxer, *Proc. Natl. Acad. Sci. USA* **2009**, *106*, 979.

[19] S. Deshpande, S. Wunnava, D. Hueting, C. Dekker, *Small* **2019**, *15*, 1902898.

[20] R. B. Lira, T. Robinson, R. Dimova, K. A. Riske, *Biophys. J.* **2019**, *116*, 79.

[21] S. Deshpande, F. Brandenburg, A. Lau, M. G. F. Last, W. K. Spoelstra, L. Reese, S. Wunnava, M. Dogterom, C. Dekker, *Nat. Commun.* **2019**, *10*, 1800.

[22] N. Yandrapalli, J. Petit, O. Bäumchen, T. Robinson, *Commun. Chem.* **2021**, *4*, 100.

[23] J. W. Hindley, Y. Elani, C. M. McGilvery, S. Ali, C. L. Bevan, R. V. Law, O. Ces, *Nat. Commun.* **2018**, *9*, 1093.

[24] M. J. Booth, V. R. Schild, A. D. Graham, S. N. Olof, H. Bayley, *Sci. Adv.* **2016**, *2*, e1600056.

[25] E. H. Reed, B. S. Schuster, M. C. Good, D. A. Hammer, *ACS Synth. Biol.* **2020**, *9*, 500.

[26] C. Chou, D. Young, A. Deiters, *Angew. Chem., Int. Ed.* **2009**, *48*, 5950.

[27] K. Jahnke, M. Weiss, C. Weber, I. Platzman, K. Göpfrich, J. P. Spatz, *Adv. Biosyst.* **2020**, *4*, 2000102.

[28] K. Jahnke, N. Ritzmann, J. Fichtler, A. Nitschke, Y. Dreher, T. Abele, G. Hofhaus, I. Platzman, R. R. Schröder, D. J. Müller, J. P. Spatz, K. Göpfrich, *Nat. Commun.* **2021**, *12*, 3967.

[29] J.-C. Lin, C.-Y. Chien, C.-L. Lin, B.-Y. Yao, Y.-I. Chen, Y.-H. Liu, Z.-S. Fang, J.-Y. Chen, W.-y. Chen, N.-N. Lee, H.-W. Chen, C.-M. J. Hu, *Nat. Commun.* **2019**, *10*, 1057.

[30] C. Campillo, B. Pépin-Donat, A. Viallat, *Soft Matter* **2007**, *3*, 1421.

[31] S. Maruo, O. Nakamura, S. Kawata, *Opt. Lett.* **1997**, *22*, 132.

[32] X. Zheng, J. Deotte, M. P. Alonso, G. R. Farquar, T. H. Weisgraber, S. Gemberling, H. Lee, N. Fang, C. M. Spadaccini, *Rev. Sci. Instrum.* **2012**, *83*, 125001.

[33] V. Hahn, P. Kiefer, T. Frenzel, J. Qu, E. Blasco, C. Barner-Kowollik, M. Wegener, *Adv. Funct. Mater.* **2020**, *30*, 1907795.

[34] M. Hippler, E. Blasco, J. Qu, M. Tanaka, C. Barner-Kowollik, M. Wegener, M. Bastmeyer, *Nat. Commun.* **2019**, *10*, 232.

[35] D. Jin, Q. Chen, T.-Y. Huang, J. Huang, L. Zhang, H. Duan, *Mater. Today* **2020**, *32*, 19.

[36] J. Torgersen, X.-H. Qin, Z. Li, A. Ovsianikov, R. Liska, J. Stampfl, *Adv. Funct. Mater.* **2013**, *23*, 4542.

[37] B. Kaehr, J. B. Shear, *Proc. Natl. Acad. Sci. USA* **2008**, *105*, 8850.

[38] J. Torgersen, A. Ovsianikov, V. Mironov, N. Pucher, X. Qin, Z. Li, K. Cicha, T. Machacek, R. Liska, V. Jantsch, J. Stampfl, *J. Biomed. Opt.* **2012**, *17*, 105008.

[39] J. Song, C. Michas, C. S. Chen, A. E. White, M. W. Grinstaff, *Macromol. Biosci.* **2021**, *21*, 2100051.

[40] W. Zhang, P. Soman, K. Meggs, X. Qu, S. Chen, *Adv. Funct. Mater.* **2013**, *23*, 3226.

[41] S. Engelhardt, E. Hoch, K. Borchers, W. Meyer, H. Krüger, G. E. M. Tovar, A. Gillner, *Biofabrication* **2011**, *3*, 025003.

[42] R. Dimova, *Annu. Rev. Biophys.* **2019**, *48*, 93.

[43] E. Rideau, R. Dimova, P. Schwille, F. R. Wurm, K. Landfester, *Chem. Soc. Rev.* **2018**, *47*, 8572.

[44] T. J. Lagny, P. Bassereau, *Interface Focus* **2015**, *5*, 20150038.

[45] R. Mau, J. Nazir, S. John, H. Seitz, *Curr. Dir. Biomed. Eng.* **2019**, *5*, 249.

[46] M. Malinauskas, P. Danilevičius, D. Baltriukienė, M. Rutkauskas, A. Žukauskas, Ž. Kairytė, G. Bičkauskaitė, V. Purlys, D. Paipulas, V. Bukelskienė, R. Gadonas, *Lith. J. Phys.* **2010**, *50*, 75.

[47] J. Cama, M. Schaich, K. Al Nahas, S. Hernández-Ainsa, S. Pagliara, U. F. Keyser, *Sci. Rep.* **2016**, *6*, 32824.

[48] P. K. Gasbjerg, P. A. Knauf, J. Brahm, *J. General Physiol.* **1996**, *108*, 565.

[49] H. Sauer, V. Pütz, K. Fischer, J. Hescheler, M. Wartenberg, *Br. J. Cancer* **1999**, *80*, 1204.

[50] H. Ko, M. C. Ratri, K. Kim, Y. Jung, G. Tae, K. Shin, *Sci. Rep.* **2020**, *10*, 7527.

[51] C. N. LaFratta, J. T. Fourkas, T. Baldacchini, R. A. Farrer, *Angew. Chem., Int. Ed.* **2007**, *46*, 6238.

[52] R. Wood, F. Wirth, H. Morgan, *Biochim. Biophys. Acta, Biomembr.* **1968**, *163*, 171.

[53] B. Alberts, D. Bray, J. Lewis, M. Raff, K. Roberts, J. D. Watson, *Molecular Biology of the Cell*, 5th ed., Garland Science, New York **2008**.

[54] T. Abele, T. Messer, K. Jahnke, M. Hippler, M. Bastmeyer, M. Wegener, K. Göpfrich, 2021, "Two-Photon 3D laser Printing Inside Synthetic Cells [Research Data]", heiDATA, 1.0, https://doi.org/10.11588/data/PUKJCV.